Theoretical Study of Photoinduced Proton-Coupled Electron Transfer through Asymmetric Salt Bridges

Alexander Soudackov and Sharon Hammes-Schiffer*

Contribution from the Department of Chemistry and Biochemistry, University of Notre Dame, Notre Dame, Indiana 46556-5670

Received July 8, 1999

Abstract: The theoretical study in this paper is based on the experimental result that the rate of photoinduced electron transfer is $\sim 10^2$ times slower through a donor−(amidinium−carboxylate)−acceptor salt bridge than through the corresponding switched interface donor−(carboxylate−amidinium)−acceptor complex (Kirby, J. P.; Roberts, J. A.; Nocera, D. G. *J. Am. Chem. Soc.* **1997**, *119*, 9230). This experimental result indicates that the proton-transfer interface plays an important role in these electron-transfer reactions. In this paper, a multistate continuum theory for proton-coupled electron transfer (PCET) is applied to analogues representing the chemical systems studied in these experiments. The solute is described with a multistate valence bond model, the solvent is represented as a dielectric continuum, and the active electrons and transferring proton(s) are treated quantum mechanically on equal footing. The application of this theory to these PCET systems provides adiabatic free energy surfaces that depend on two scalar solvent variables corresponding to the proton and electron transfer reactions. The theoretical analysis indicates that the experimentally observed difference in rates for the two chemical systems is due to differences in solute electrostatic properties, solvation energies, solvent reorganization energies, and electronic couplings. Moreover, this theoretical study provides insight into the underlying fundamental principles of PCET reactions.

Introduction

Proton-coupled electron transfer (PCET) reactions play a vital role in a variety of biological processes, including photosynthesis[1] and respiration.[2] To elucidate the relationship between electron transfer and proton motion, Nocera and co-workers developed an experimental approach to photoinduce electron transfer within an electron donor−accepor pair juxtaposted by a proton transfer interface.[3−5] The theoretical study in this paper is based on experiments that directly compare the rate of electron transfer through a donor−(amidinium−carboxylate)−acceptor salt bridge and the corresponding switched interface donor−(carboxylate−amidinium)−acceptor complex. In the experimentally studied systems **1** and **2**, the donor is $[(tmbpy)_2Ru^{II}(Mebpy\text{-}amH^+)]^{3+}$ or $[(tmbpy)_2Ru^{II}(Mebpy\text{-}COO^-)]^+$ (where tmbpy = 3,3′,4,4′-tetramethyl-2,2′-bipyridine, Mebpy-amH$^+$ = 4-methyl-2,2′-bipyridine-4′-amidinium, Mebpy-COO$^-$ = 4-methyl-2,2′-bipyridine-4′-carboxylate), and the acceptor is the complementary carboxylate- or amidinium-modified 3,5-dinitrobenzene. Such amidinium−carboxylate interfaces are related to the aspartate−arginine salt bridges found in a range of biological systems, including RNA, DNA complexes, and enzymes.[6]

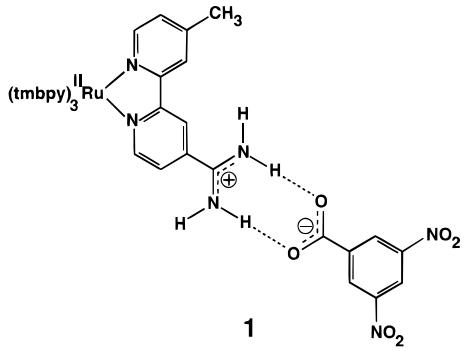

1

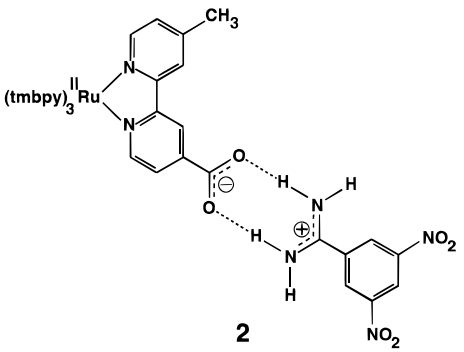

2

* Corresponding author: (e-mail) hammes-schiffer.1@nd.edu.

(1) Babcock, G. T.; Barry, B. A.; Debus, R. J.; Hoganson, C. W.; Atamian, M.; McIntosh, L.; Sithole, I.; Yocum, C. F. *Biochemistry* **1989**, *28*, 9557. Okamura, M. Y.; Feher, G. *Annu. Rev. Biochem.* **1992**, *61*, 861. Kirmaier, C.; Holten, D. *The Photosynthetic Bacterial Reaction Center: Structure and Dynamics*; Plenum: New York, 1988.

(2) Wikstrom, M. *Nature* **1989**, *338*, 776. Babcock, G. T.; Wikstrom, M. *Nature* **1992**, *356*, 301. Malmstrom, B. G. *Acc. Chem. Res.* **1993**, *26*, 332.

(3) Turro, C.; Chang, C. K.; Leroi, G. E.; Cukier, R. I.; Nocera, D. G. *J. Am. Chem. Soc.* **1992**, *114*, 4013.

(4) Roberts, J. A.; Kirby, J. P.; Nocera, D. G. *J. Am. Chem. Soc.* **1995**, *117*, 8051.

(5) Kirby, J. P.; Roberts, J. A.; Nocera, D. G. *J. Am. Chem. Soc.* **1997**, *119*, 9230.

10.1021/ja992380y CCC: $18.00
Published on Web 10/27/1999

Nocera and co-workers synthesized complexes **1** and **2** and initiated the electron transfer reaction by laser excitation of the metal-to-ligand charge-transfer (MLCT) transition of the Ru(II) polypyridyl complex. This photoexcitation cleanly promotes the transferring electron to the Mebpy ligand, from where it is transferred to the dinitrobenzoic acceptor through the salt bridge interface. The rates of PCET through the amidinium−carboxylate and carboxylate−amidinium interfaces were found to be 8.4×10^6 and 3.1×10^8 s^{-1}, respectively, for **1** and **2**. This substantial difference between the rates for the two systems indicates that the proton transfer interface plays a significant role in the electron transfer reactions.

Two different theoretical formulations for PCET in solution have been proposed in the literature. The first was developed by Cukier and co-workers and has been applied to a range of simple model systems.[7] This paper focuses on the second formulation, which was developed by the present authors as a specific case of a multistate continuum theory[8,9] for multiple charge transfer reactions in solution.[10] In this theory, the solute is described with a multistate valence bond (VB) model,[11−13] the solvent is represented as a dielectric continuum, and the active electrons and transferring proton(s) are treated quantum mechanically on equal footing. This theory provides adiabatic free energy surfaces that depend on a set of scalar solvent variables corresponding to the individual charge transfer reactions. Thus, this theory is a multidimensional analogue of standard Marcus theory for outer-sphere electron transfer reactions.[14] The input quantities required for this theory are gas phase valence bond matrix elements represented as molecular mechanical terms fit to electronic structure calculations and solvent reorganization energy matrix elements obtained with standard electrostatic continuum methods.[15]

In this paper, we apply our theoretical formulation for PCET to analogues of the experimentally studied systems **1** and **2**. Our electronic structure calculations performed on the electron donor $[(tmbpy)_2Ru^{II}(Mebpy\text{-}amH^+)]^{3+}$ indicate that photoexcitation from the highest occupied molecular orbital (HOMO) to the lowest unoccupied molecular orbital (LUMO) promotes an electron from a Ru d-orbital to the Mebpy-amH$^+$ ligand, consistent with the experimental observations. Since the Ru center and the two tmbpy ligands are not expected to significantly affect the mechanism of the PCET reaction after photoexcitation, for simplicity they are removed for our calculations. The resulting systems are denoted as DNOA for the analogue of **1** and DONA for the analogue of **2**. Note that DNOA and DONA are negatively charged to represent the complex after photoexcitation (i.e., after the MLCT transition). The unpaired electron is the active electron in the PCET reaction.

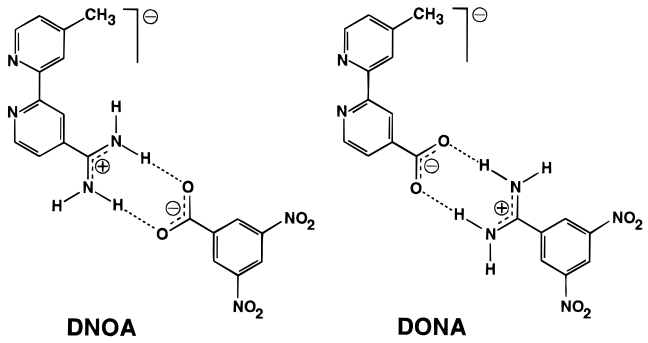

An outline of the paper is as follows. First, we summarize our multistate continuum theory for PCET and outline the prescription for obtaining the required input quantities. Then, we present the results of the application of this methodology to DNOA and DONA. Finally, we summarize the differences between the results for the two systems and discuss how these differences provide insight into the experimental observations.

Theory and Methods

Multistate Continuum Theory for PCET. Reference 10 presents the detailed derivation of our multistate continuum theory for PCET reactions in solution. In this section, we briefly summarize the results from this previous paper. The PCET system is represented by a four-state VB model with electronic VB states defined as

$$\begin{aligned}
&(1a)\quad D_e^- - {}^+D_p\,H \cdots \cdots A_p^- - A_e \\
&(1b)\quad D_e^- - D_p \cdots \cdots H\,A_p - A_e \\
&(2a)\quad D_e - {}^+D_p\,H \cdots \cdots A_p^- - A_e^- \\
&(2b)\quad D_e - D_p \cdots \cdots H\,A_p - A_e^- \qquad (1)
\end{aligned}$$

Here the symbols D_e and A_e represent a general electron donor and acceptor, D_p and A_p represent a general proton donor and acceptor, and H represents the transferring proton. (In this paper we include only two charge transfer reactions, but the theoretical formulation is easily extendable to the general situation with any number of charge transfer reactions.) The VB states are labeled as follows: *a* denotes that the proton is bonded to its donor while *b* denotes that the proton is bonded to its acceptor, and 1 denotes that the electron is localized on its donor while 2 denotes that the electron is localized on its acceptor. Thus, *a* and *b* indicate the proton transfer (PT) state, and 1 and 2 indicate the electron transfer (ET) state. The solvent is represented as a dielectric continuum characterized by the electronic and inertial dielectric constants ϵ_∞ and ϵ_o, respectively. The active electrons and transferring proton are treated quantum mechanically on equal footing. Reference 10 provides a prescription for calculating the mixed electronic/proton vibrational adiabatic states as functions of two scalar solvent coordinates z_p and z_e corresponding to the proton and electron transfer reactions, respectively. Each scalar solvent coordinate represents the difference in interaction energy of the two VB states involved in the charge transfer reaction with the inertial polarization field $\phi_{in}(\mathbf{r})$ of the solvent. Thus,

$$z_p = \int d\mathbf{r}[\rho_{1b,1b}(\mathbf{r}) - \rho_{1a,1a}(\mathbf{r})]\phi_{in}(\mathbf{r})$$

(6) Ramirez, B. E.; Malmstrom, B. G.; Winkler, J. R.; Gray, H. B. *Proc. Natl. Acad. Sci. U.S.A.* **1995**, *92*, 11949. Brzezinski, P. *Biochemistry* **1996**, *35*, 5611. Puglisi, J. D.; Chen, L.; Frankel, A. D.; Williamson, J. R. *Proc. Natl. Acad. Sci. U.S.A.* **1993**, *90*, 3680. Berg, J. M. *Acc. Chem. Res.* **1995**, *28*, 14. Howell, E. E.; Villafranca, J. E.; Warren, M. S.; Oatley, S. J.; Kraut, J. *Science* **1986**, *231*, 1125. Crane, B. R.; Siegel, L. M.; Getzoff, E. D. *Science* **1995**, *270*, 59.

(7) Cukier, R. I. *J. Phys. Chem.* **1994**, *98*, 2377. Zhao, X. G.; Cukier, R. I. *J. Phys. Chem.* **1995**, *99*, 945. Cukier, R. I. *J. Phys. Chem.* **1995**, *99*, 16101. Cukier, R. I. *J. Phys. Chem.* **1996**, *100*, 15428.

(8) Bianco, R.; Hynes, J. T. *J. Chem. Phys.* **1995**, *102*, 7864. Bianco, R.; Hynes, J. T. *J. Chem. Phys.* **1995**, *102*, 7885.

(9) Basilevsky, M. V.; Chudinov, G. E.; Newton, M. D. *Chem. Phys.* **1994**, *179*, 263.

(10) Soudackov, A. V.; Hammes-Schiffer, S. *J. Chem. Phys.* **1999**, *111*, 4672.

(11) Warshel, A. *Computer Modeling of Chemical Reactions in Enzymes and Solutions*; John Wiley: New York, 1991.

(12) Vuilleumier, R.; Borgis, D. *Chem. Phys. Lett.* **1998**, *284*, 71.

(13) Schmitt, U.; Voth, G. A. *J. Phys. Chem. B* **1998**, *102*, 5547.

(14) Marcus, R. A. *J. Chem. Phys.* **1956**, *24*, 966. Marcus, R. A. *J. Chem. Phys.* **1965**, *43*, 679. Marcus, R. A. *Annu. Rev. Phys. Chem.* **1964**, *15*, 155.

(15) Tomasi, J.; Persico, M. *Chem. Rev.* **1994**, *94*, 2027.

$$z_e = \int d\mathbf{r}[\rho_{2a,2a}(\mathbf{r}) - \rho_{1a,1a}(\mathbf{r})]\phi_{in}(\mathbf{r}) \quad (2)$$

where $\rho_{ii}(\mathbf{r})$ is the total charge density of VB state i. These scalar solvent coordinates are analogous to the standard solvent coordinate used for the description of single charge transfer reactions.[16,17]

The approach used in this paper for calculating the mixed electronic/proton vibrational adiabatic states consists of three steps. The first step is to calculate the energies of the electronic diabatic states for fixed solvent coordinates (z_p,z_e) for all points r_p along a one-dimensional grid between the proton donor and acceptor. The energy of the diabatic electronic state i is

$$E_i^{(dia)}(r_p,z_p,z_e) = S(r_p,z_p,z_e) + H_{ii}(r_p,z_p,z_e) \quad (3)$$

Here the transformed self-energy of the inertial polarization field is

$$S(r_p,z_p,z_e) = \frac{1}{2}\sum_{i,j=1b,2a}\{[y'_i + t'_{1a,i}(r_p)] \times [\mathbf{t}'_t(r_p)^{-1}]_{i,j}[y'_j + t'_{1a,j}(r_p)]\} - \frac{1}{2}t'_{1a,1a}(r_p) \quad (4)$$

where the summation runs over valence bond states 1b and 2a, the truncated reorganization energy matrix $\mathbf{t}'_t$ has dimensions 2 × 2 corresponding to these two states, and $(z_p,z_e) \equiv (y'_{1b},y'_{2a})$. (As shown in ref 10, the 1a state is eliminated through a coordinate transformation and the 2b state is eliminated due to a linear dependency among the solvent coordinates.) The inertial reorganization energy matrix elements t'_{ij} can be expressed as

$$t'_{ij} = -\int d\mathbf{r}\, \nu_{jj}(\mathbf{r})[\hat{K}(\epsilon_o) - \hat{K}(\epsilon_\infty)]\nu_{ii}(\mathbf{r}) \quad (5)$$

where $\hat{K}(\epsilon)$ is the dielectric Green function[18] for the medium with dielectric constant ϵ and

$$\nu_{1a,1a}(\mathbf{r}) = \rho_{1a,1a}(\mathbf{r})$$
$$\nu_{ii}(\mathbf{r}) = \rho_{ii}(\mathbf{r}) - \rho_{1a,1a}(\mathbf{r}) \qquad (i = 1b,2a,2b) \quad (6)$$

(Note that $\nu_{ii}(\mathbf{r})$ and $\rho_{ii}(\mathbf{r})$ depend on the position r_p of the transferring hydrogen atom, but for notational simplicity, this dependence will be omitted from the equations in this paper.) Furthermore, $H_{ii}(r_p,z_p,z_e)$ is the diagonal matrix element of the matrix

$$\mathbf{H}(r_p,z_p,z_e) = \begin{pmatrix} (H_o)_{1a,1a} & (H_o)_{1a,1b} & (H_o)_{1a,2a} & (H_o)_{1a,2b} \\ (H_o)_{1b,1a} & (H_o)_{1b,1b} + z_p & (H_o)_{1b,2a} & (H_o)_{1b,2b} \\ (H_o)_{2a,1a} & (H_o)_{2a,1b} & (H_o)_{2a,2a} + z_e & (H_o)_{2a,2b} \\ (H_o)_{2b,1a} & (H_o)_{2b,1b} & (H_o)_{2b,2a} & (H_o)_{2b,2b} + z_p + z_e \end{pmatrix} \quad (7)$$

Here

$$(H_o)_{ij}(r_p) = (h_o)_{ij}(r_p) - \frac{1}{2}t_{ii}^{(\infty)}(r_p)\delta_{ij} \quad (8)$$

where $(h_o)_{ij}(r_p)$ is the gas-phase matrix element and

$$t_{ij}^{(\infty)}(r_p) = -\int d\mathbf{r}\, \rho_{jj}(\mathbf{r})\hat{K}(\epsilon_\infty)\rho_{ii}(\mathbf{r}) \quad (9)$$

is the electronic reorganization energy matrix element between VB states i and j. Note that in this paper we are assuming that the solvent electrons are infinitely fast on the time scale of the solute electrons (i.e., the Born−Oppenheimer limit for electron transfer[19]).

The second step of this prescription is to calculate the proton vibrational adiabatic states $\phi_\mu^{(i)}(r_p;\, z_p,z_e)$ for fixed solvent coordinates for each diabatic electronic state i by numerically solving the one-dimensional Schrödinger equation

$$\left(-\frac{\hbar^2}{2m_p}\frac{\partial^2}{\partial r_p^2} + E_i^{(dia)}\right)\phi_\mu^{(i)}(r_p;z_p,z_e) = \epsilon_\mu^{(i)}(z_p,z_e)\phi_\mu^{(i)}(r_p;z_p,z_e) \quad (10)$$

In this paper, we solve this equation by expanding the proton vibrational states on a grid along the axis between the proton donor and acceptor and implementing standard discrete Fourier grid techniques.

The third step in this approach is to calculate the numerically exact mixed electronic/proton vibrational adiabatic states by expanding them in terms of basis states, each composed of a product of an electronic diabatic state i and a proton vibrational adiabatic state $\phi_\mu^{(i)}$. The mixed electronic/vibrational states are calculated by solving the matrix equation

$$\mathbf{H}'\mathbf{D} = \mathbf{D}\mathbf{E} \quad (11)$$

where $\mathbf{D}$ has elements $D_{i\mu,n}$, $\mathbf{E}$ is diagonal with elements E_n, and the matrix elements of the Hamiltonian $\mathbf{H}'$ are

$$H'_{i\mu,j\nu} = \delta_{ij}\delta_{\mu\nu}\epsilon_\mu^{(i)}(z_p,z_e) + (1-\delta_{ij})\langle\phi_\mu^{(i)}|H_{ij}|\phi_\nu^{(j)}\rangle_p \quad (12)$$

(Here, $\langle\ \rangle_p$ indicates integration over r_p.) The energies of the mixed electronic/proton vibrational adiabatic states can be calculated as functions of the two scalar solvent variables z_p and z_e by following these three steps for solvent coordinates $(z_p,\, z_e)$ on a two-dimensional grid.

The derivation of a general analytical rate expression for PCET is a challenging theoretical problem that has not yet been solved. To obtain an approximate rate for PCET reactions, we can utilize the standard rate expression[14,20] for nonadiabatic electron transfer along a straight-line reaction path for each pair of interacting *electronically diabatic* states in our two-dimensional description. The resulting rate expression can be written in the form

$$k = \frac{2\pi}{\hbar}\sum_m \rho_m \sum_n (4\pi\lambda_{mn}k_BT)^{-1/2}|V_{mn}|^2 \times \exp[-(\Delta G^\circ_{mn} + \lambda_{mn})^2/(4\lambda_{mn}k_BT)] \quad (13)$$

Here m and n denote the mixed electronic/proton vibrational adiabatic wave functions $\Phi_m(\mathbf{r}_e,r_p)$ and $\Phi_n(\mathbf{r}_e,r_p)$ obtained with $(h_o)_{ij} = 0$ if i and j represent different ET states (i.e., diabatic with respect to ET and adiabatic with respect to PT). The electronic parts of the states Φ_m are mixtures of VB states 1a and 1b, while those of the states Φ_n are mixtures of VB states 2a and 2b. In eq 13, ρ_m is the probability of being in reactant state m (i.e., the normalized Boltzmann factor), λ_{mn} is the solvent reorganization energy for states m and n, ΔG°_{mn} is the free energy difference between states m and n, and $V_{mn} = \langle\Phi_m|H|\Phi_n\rangle_{ep}$ is the coupling between states m and n evaluated at the point of intersection of states m and n (where the brackets indicate

(16) Zusman, L. D. *Chem. Phys.* **1980**, *49*, 295.
(17) Calef, D. F.; Wolynes, P. G. *J. Phys. Chem.* **1983**, *87*, 3387.
(18) Newton, M. D.; Friedman, H. L. *J. Chem. Phys.* **1988**, *88*, 4460. Liu, Y.-P.; Newton, M. D. *J. Phys. Chem.* **1995**, *99*, 12382.
(19) Kim, H. J.; Hynes, J. T. *J. Chem. Phys.* **1992**, *96*, 5088−5110.
(20) Levich, V. G. *Adv. Electrochem. Electrochem. Eng.* **1966**, *4*, 249.

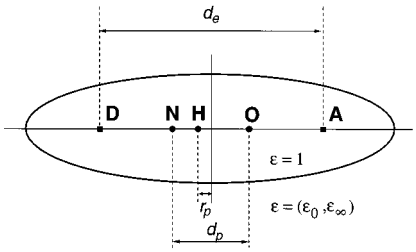

Figure 1. Ellipsoidal continuum model used in the electrostatic calculations of the solvation quantities. The point charge sites are shown here for DNOA; those for DONA are the same except the N and O are interchanged.

integration over both the electronic and proton vibrational coordinates and H is the total Hamiltonian of the system).

We emphasize that eq 13 is an *approximate* expression for the rate. The standard rate expression[21−23] used here is based on the assumptions that the electron transfer is nonadiabatic ($V_{mn} \ll kT$) and the solvent relaxation is fast enough to maintain a Boltzmann distribution in the reactant well. The main additional approximation invoked in our application of eq 13 to PCET is that the reaction path is assumed to be a straight line along a single solvent reaction coordinate. Typically this assumption is valid if the coupling between the solvent and the PT reaction is significantly weaker than the coupling between the solvent and the ET reaction. Our analysis of the two-dimensional adiabatic free energy surfaces for the systems studied in this paper suggests that this assumption is reasonable for these systems. Currently we are directing our efforts toward deriving a new rate expression for general PCET reactions.

Calculation of Input Quantities. The input quantities required for the theory described above are the gas phase valence bond matrix elements and the reorganization energy matrix elements. In this paper, the charge density of each valence bond state is described by a set of five point charges representing the electron donor and acceptor, the proton donor and acceptor, and the transferring hydrogen atom. (As discussed above, although the amidinium−carboxylate proton transfer interfaces of these systems contain two nearly equivalent NH−O hydrogen bonds, only one proton is expected to transfer during the PT reaction. Thus, in this paper only one proton transfer reaction is considered.) These sites are arranged as shown in Figure 1.

The matrix elements of the gas phase Hamiltonian h_o are approximated by standard molecular mechanical terms fit to electronic structure calculations for the gas phase solute. In this paper, the diagonal matrix elements of the gas phase Hamiltonian are expressed as

$$(h_o)_{1a1a}(r_p) = U_{NH}^{Morse}(r_p) + U_{OH}^{rep}(r_p) + U_{1a}^{Coul}(r_p)$$

$$(h_o)_{1b1b}(r_p) = U_{OH}^{Morse}(r_p) + U_{NH}^{rep}(r_p) + U_{1b}^{Coul}(r_p) + \Delta_{1b}$$

$$(h_o)_{2a2a}(r_p) = U_{NH}^{Morse}(r_p) + U_{OH}^{rep}(r_p) + U_{2a}^{Coul}(r_p) + \Delta_{2a}$$

$$(h_o)_{2b2b}(r_p) = U_{OH}^{Morse}(r_p) + U_{NH}^{rep}(r_p) + U_{2b}^{Coul}(r_p) + \Delta_{2b} \quad (14)$$

where

$$U_{AH}^{Morse}(r_p) = D_{AH}(1 - e^{-\beta_{AH}(R_{AH}-R_{AH}^{\circ})})^2 \quad (15)$$

is a Morse potential for an A−H bond,

$$U_{AH}^{rep}(r_p) = D'_{AH}e^{-\beta'_{AH}R_{AH}} \quad (16)$$

is a repulsion term between nonbonded atoms A and H, and

$$U_i^{Coul}(r_p) = \frac{1}{2}\sum_{k\neq l}\frac{q_k^i q_l^i}{R_{kl}} \quad (17)$$

is a Coulomb interaction potential between the point charges illustrated in Figure 1 (where the summation is over sites k, l and q_k^i is the charge on site k for VB state i). In all of these expressions, R_{kl} is the distance between sites k and l. In this paper, the couplings between the VB states are assumed to be constant:

$$(h_o)_{1a,1b} = V^{PT1}$$

$$(h_o)_{2a,2b} = V^{PT2}$$

$$(h_o)_{1a,2a} = (h_o)_{1b,2b} = V^{ET}$$

$$(h_o)_{1a,2b} = (h_o)_{1b,2a} = V^{EPT} \quad (18)$$

The parameters entering all of these molecular mechanical expressions were fit to the electronic structure calculations discussed below. The electronic structure calculations described in this paper were performed with GAUSSIAN98.[25]

The reorganization energy matrix elements are calculated with a simple electrostatic ellipsoidal model developed by Kirkwood and Westheimer[24] and used recently by Cukier[7] for similar systems. In this model, the point charges representing the solute charge distribution for each VB state are placed on the main axis of an ellipsoidal cavity embedded in a dielectric continuum solvent characterized by the inertial (ϵ_0) and optical (ϵ_∞) dielectric constants. (See Figure 1 for a schematic illustration.) For this simple model, the electrostatic equations for the polarization potentials can be solved analytically. Thus, exact expressions can be used to calculate the solvation energies and reorganization energy matrix elements.

Results and Discussion

Gas-Phase Quantities. In the formulation described above, the matrix elements of the gas phase Hamiltonian are fit to electronic structure calculations of the gas phase reaction complex. As described in eq 1, the four VB states are 1*a*, 1*b*, 2*a*, and 2*b*, where *a* and *b* indicate the PT state, and 1 and 2 indicate the ET state. For both systems, *a* denotes that the proton is bonded to the amidinium while *b* denotes that the proton is bonded to the carboxylate of the PT interface, and 1 denotes that the electron is localized on the electron donor Mebpy while

(21) Jortner, J. *J. Chem. Phys.* **1976**, *64*, 4860.
(22) Newton, M. D.; Sutin, N. *Annu. Rev. Phys. Chem.* **1984**, *35*, 437.
(23) Barbara, P. F.; Meyer, T. J.; Ratner, M. A. *J. Phys. Chem.* **1996**, *100*, 13148.
(24) Westheimer, F. H.; Kirkwood, J. G. *J. Chem. Phys.* **1938**, *6*, 513.
(25) Gaussian 98, Revision A.6, Frisch, M. J.; Trucks, G. W.; Schlegel, H. B.; Scuseria, G. E.; Robb, M. A.; Cheeseman, J. R.; Zakrzewski, V. G.; Montgomery, J. A., Jr.; Stratmann, R. E.; Burant, J. C.; Dapprich, S.; Millam, J. M.; Daniels, A. D.; Kudin, K. N.; Strain, M. C.; Farkas, O.; Tomasi, J.; Barone, V.; Cossi, M.; Cammi, R.; Mennucci, B.; Pomelli, C.; Adamo, C.; Clifford, S.; Ochterski, J.; Petersson, G. A.; Ayala, P. Y.; Cui, Q.; Morokuma, K.; Malick, D. K.; Rabuck, A. D.; Raghavachari, K.; Foresman, J. B.; Cioslowski, J.; Ortiz, J. V.; Stefanov, B. B.; Liu, G.; Liashenko, A.; Piskorz, P.; Komaromi, I.; Gomperts, R.; Martin, R. L.; Fox, D. J.; Keith, T.; Al-Laham, M. A.; Peng, C. Y.; Nanayakkara, A.; Gonzalez, C.; Challacombe, M.; Gill, P. M. W.; Johnson, B.; Chen, W.; Wong, M. W.; Andres, J. L.; Gonzalez, C.; Head-Gordon, M.; Replogle, E. S.; Pople, J. A., Gaussian, Inc., Pittsburgh, PA, 1998.

2 denotes that the electron is localized on the electron acceptor dinitrobenzene.

We performed electronic structure calculations to obtain the adiabatic energies of the two active electronic states along the transferring proton coordinate r_p for the DNOA and DONA systems in the gas phase. As mentioned above, although the amidinium−carboxylate proton transfer interface of the reaction complex contains two nearly equivalent hydrogen bonds, only one proton is expected to transfer during the PT reaction. For our calculations, we consider only the PT reaction with the lower potential barrier and assume that this transferring proton moves in one dimension along the N−O internuclear axis (with coordinate r_p represented on a one-dimensional grid). This proton is the lower proton in the illustrations of DNOA and DONA shown in the Introduction. For simplicity, the position of the other proton is assumed to be fixed. In future calculations, we will investigate the effects of treating both protons equivalently.

The geometries for DNOA and DONA were obtained at the RHF/6-31G** level according to the following procedure. First we optimized separate groups representing the electron donor and acceptor, i.e., Mebpy-amH$^+$ and dinitrobenzene-COO$^-$ for DNOA and Mebpy-COO$^-$ and dinitrobenzene-amH$^+$ for DONA. These optimizations were constrained to planar geometries since planar configurations of the reaction complex provide the maximum overlap between the donor and acceptor orbitals and thus the maximum electronic coupling strength. Then we combined the electron donor and acceptor groups (with the geometries of the Mebpy and dinitrobenzene groups frozen) and optimized the geometry of the salt bridge in the PT state *a*, maintaining planarity for the electron donor−acceptor system. (We found that releasing these planar constraints did not qualitatively alter the final results.) Our results indicate that the N−O bond lengths are 2.696 and 2.631 Å for DNOA and DONA, respectively, indicating a stronger hydrogen bond in DONA. Note that the geometries were obtained for the neutral complex to avoid inconsistencies between DNOA and DONA since, for the negatively charged complex, the electron is localized on the donor for DNOA and on the acceptor for DONA in the ground electronic state of PT state *a*. All further calculations were performed for the negatively charged complex.

In this paper, all solute nuclei except the transferring proton are assumed to be fixed during the reaction. Thus, the reactions are assumed to be dominated by outer-sphere (i.e., solvent) reorganization. To estimate the importance of inner-sphere reorganization for these systems, we performed additional electronic structure calculations on DNOA. First, we optimized both the neutral and negatively charged forms of the separate protonated groups representing the electron donor and acceptor, i.e., Mebpy-amH$^+$, Mebpy$^-$-amH$^+$, dinitrobenzene-COOH, and dinitrobenzene$^-$-COOH, maintaining planarity as described above. Then, we combined the geometries of neutral and negatively charged Mebpy and dinitrobenzene obtained from these calculations to create two complexes: the geometry of Mebpy with that of dinitrobenzene$^-$ and the geometry of Mebpy$^-$ with that of dinitrobenzene. When the geometry of the PT interface was set to that obtained for the neutral complex with the PT state *a* for both complexes, the electron was localized on the electron donor, representing ET state 1. In this case, we found the difference in energies between these two complexes to be 13.8 kcal/mol. When the geometry of the PT interface was set to that for the neutral complex with the PT state *b* for both complexes, the electron was localized on the electron acceptor, representing ET state 2. In this case, we found the difference in energies between these two complexes to be 11.0 kcal/mol. In these calculations we are assuming that the position of the transferring proton has a negligible effect on the inner-sphere reorganization energy of the complex. This assumption is validated by the similarity of the results for PT states *a* and *b*. Thus, the inner-sphere reorganization energy for this complex is ∼12.5 kcal/mol, which is ∼30% of the outer-sphere reorganization energy for these systems. In this paper, the inner-sphere reorganization is neglected for simplicity. Future work will include the inner-sphere reorganization in our multistate continuum theory as described in ref 10.

We calculated the adiabatic energies along the proton coordinate with the state-averaged (SA) CASSCF method at the 6-31G** level. We obtained the initial molecular orbitals (MOs) for the CASSCF calculations by performing ROHF/6-31G** calculations for the doublet state with the proton located at each point along a one-dimensional grid between the proton donor and acceptor. For DNOA, the active space in CASSCF was composed of two MOs localized on the acceptor site and one MO localized on the donor site. For DONA, one additional MO localized on the acceptor site was added to the active space. For both systems, only one unpaired electron (i.e., the active electron in the ET reaction) was included in the active space, so no correlation effects were taken into account. This simplification is partially justified by the fact that the highest doubly occupied MO for all grid points for both systems is well separated in energy (by ∼7 eV) from the lowest singly occupied active MO. The three lowest states for DNOA and the four lowest states for DONA were included in the state-averaging process for the CASSCF calculations. The adiabatic energies of the two active electronic states as functions of the proton position are presented in Figure 2. The two active electronic states are denoted D and A, where D corresponds to the active electron localized on the donor with a molecular orbital similar to the HOMO of the separated negatively charged electron donor Mebpy$^-$ and A corresponds to the active electron localized on the acceptor with a molecular orbital similar to the LUMO of the separated electron acceptor dinitrobenzene. The remaining states, which are localized on the acceptor, are neglected due to weak interaction with the D state. Note that in the VB notation of this paper (given in eq 1), the D state corresponds to ET state 1 and the A state corresponds to ET state 2. Moreover, the PT state *a* corresponds to the minimum with a negative proton coordinate ($r_p \sim -0.35$ Å) and the PT state *b* corresponds to the minimum with a positive proton coordinate ($r_p \sim +0.35$ Å). These adiabatic electronic energy profiles were used to fit the parameters in the expressions given above for the gas phase Hamiltonian matrix elements.

The first stage of the fitting procedure was to fit the diagonal matrix elements of the VB Hamiltonian. The point charges on the electron donor and acceptor sites are −1 and 0, respectively, for ET state 1 and are 0 and −1, respectively, for ET state 2. The point charges for the proton transfer interface sites were determined from a CHELPG analysis at the RHF/6-31G** level on the simplified system H_3C-amH$^+$−$^-$OOC-CH_3. The two PT valence bond states were distinguished in these calculations by the proton position (bonded to the amidinium for PT state *a* and to the carboxylate for PT state *b*). These calculations indicate that the charge of the transferring hydrogen atom depends only weakly on its position, so we defined the point charge of the transferring hydrogen atom to be the same (+0.55 au) for all valence bond states. The point charges on the nitrogen and oxygen atoms were obtained by summing up the CHELPG charges on all atoms of the H_3C-am and OOC-CH_3 groups,

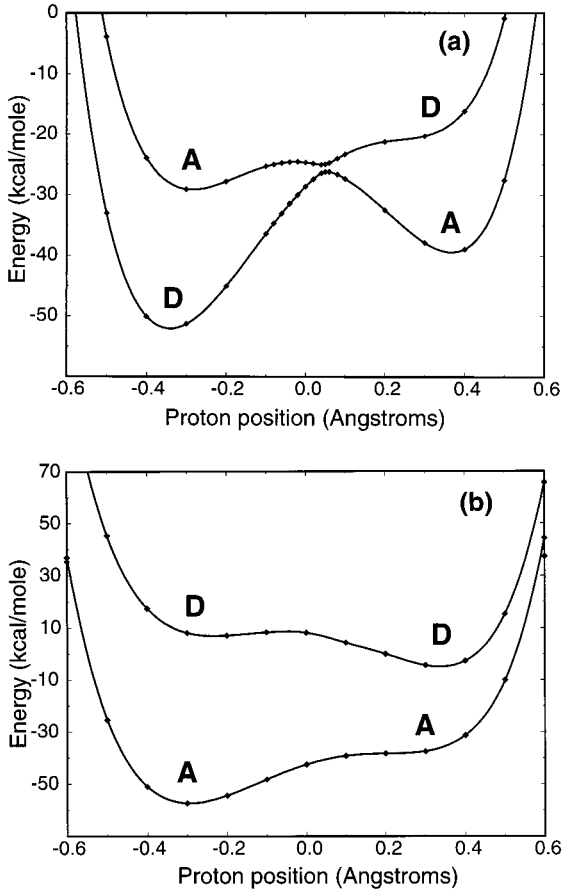

Figure 2. Gas phase energies of the active electronic adiabatic states as functions of the proton coordinate for (a) DNOA and (b) DONA. The labels D and A correspond to the active electron localized on the electron donor and acceptor, respectively.

respectively. These parameters were not altered further during the fitting procedure. Moreover, we obtained the Morse parameters from ref 11 and did not alter these in the fitting procedure. We obtained reasonable values for the repulsion parameters from ref 11 and fit these parameters, together with V^{PT1}, V^{PT2}, and the Δ_i constant terms, to the relative energies and barrier heights of the adiabatic electronic states shown in Figure 2. The values of these parameters are given in Table 1.

After this first stage of the fitting procedure was complete, the off-diagonal matrix elements of the VB Hamiltonian were determined. We used the generalized Mulliken−Hush (GMH) approach to calculate approximate values for the electronic coupling V^{ET}. In this approach,[26] the electronic matrix element V_{if} between two *diabatic* electronic states i and f is expressed in terms of the corresponding *adiabatic* state characteristics as

$$V_{if} = \frac{|\mu_{tr}|\Delta E_{ad}}{\sqrt{|\Delta\mu_{ad}|^2 + 4\mu_{tr}^2}} \qquad (19)$$

where $\Delta\mu_{ad}$ is the difference in dipole moments, μ_{tr} is the transition dipole moment, and ΔE_{ad} is the energy splitting for the adiabatic states. We used this GMH approach to estimate the electronic coupling between pairs of diabatic states 1*a*/2*a* and 1*b*/2*b* for DNOA. We performed two CI calculations at the equilibrium geometries corresponding to PT states *a* and *b* to obtain the energy splitting ΔE_{ad} and the transition dipole moment μ_{tr} between the relevant adiabatic electronic states for each PT state. We estimated $\Delta\mu_{ad}$ for each PT state using the five-site charge model described above. These calculations resulted in estimates of 0.05 and 0.08 kcal/mol for diabatic states 1*a*/2*a* and 1*b*/2*b*, respectively, for DNOA. Thus, for DNOA we approximated the electronic coupling as $V^{ET} = 0.1$ kcal/mol. We obtained the value of V^{EPT} for DNOA by fitting to the minimum splitting between the adiabatic electronic states in Figure 2a. For DONA, we calculated values of V^{ET} and V^{EPT} from the values for DNOA by assuming they are related by the factor $\exp(-\beta\Delta R/2)$, where $\beta = 1.2$ Å^{-1} (estimated from standard electron-transfer theory[27]) and $\Delta R = 0.065$ Å is the difference in N−O distances for the two systems. The values for these parameters are given in Table 1.

Table 1. The Parameters for the Gas Phase Solute EVB Model

	DNOA	DONA
D_{NH} (kcal/mol)	93.0	93.0
D_{OH} (kcal/mol)	103.0	102.0
β_{NH} (Å^{-1})	2.75	2.75
β_{OH} (Å^{-1})	2.35	2.35
R°_{NH} (Å)	1.00	1.00
R°_{OH} (Å)	0.96	0.96
D'_{NH} (kcal/mol)	2500.0	2500.0
D'_{OH} (kcal/mol)	3500.0	3500.0
β'_{NH} (Å^{-1})	3.5	3.5
β'_{OH} (Å^{-1})	3.5	3.5
Δ_{1b} (kcal/mol)	−82.0	−131.5
Δ_{2a} (kcal/mol)	5.0	−47.0
Δ_{2b} (kcal/mol)	−117.0	−149.0
V^{PT1} (kcal/mol)	50.0	60.0
V^{PT2} (kcal/mol)	55.0	60.0
V^{ET} (kcal/mol)	0.1	0.106
V^{EPT} (kcal/mol)	0.5	0.53
$q_N^{(a)}$ (au)	0.30	0.30
$q_H^{(a)}$ (au)	0.55	0.55
$q_O^{(a)}$ (au)	−0.85	−0.85
$q_N^{(b)}$ (au)	0.00	0.00
$q_H^{(b)}$ (au)	0.55	0.55
$q_O^{(b)}$ (au)	−0.55	−0.55

The calculated adiabatic energies shown in Figure 2 reveal substantial qualitative differences between DNOA and DONA. In terms of the initial ET state 1 (corresponding to the D state in Figure 2), for DNOA the 1*a* state is lower in energy than the 1*b* state, while the reverse is true for DONA. In terms of the final ET state 2 (corresponding to the A state in Figure 2), for DNOA the 2*b* state is lower in energy than the 2*a* state, while the reverse is true for DONA. Another important difference between DNOA and DONA is that DNOA exhibits an avoided crossing between the electronic states at $r_p \approx 0$, while DONA does not exhibit any avoided crossing between the electronic states for the whole range of proton coordinates. (In other words, the energy difference between ET states 1 and 2 is of opposite sign for PT states *a* and *b* for DNOA but not for DONA.) This difference suggests that the gas-phase electron transfer reaction is strongly coupled to the proton motion for DNOA but not for DONA.

Note that although the Ru atom was not included in the systems used for our calculations, the electrostatic effect of the positively charged Ru atom can be studied by including a positive charge at the location of the Ru atom. The qualitative effect of this positive charge is to lower the energies of the 1*a* and 1*b* states (i.e., the states with the electron localized on the donor) relative to those of the 2*a* and 2*b* states. Future work will include a quantitative study of the effect of the Ru atom.

(26) Newton, M. D.; Cave, R. J. *Molecular Electronics*; Blackwell Scientific: Oxford, 1997.

(27) Henderson, T. M.; Cave, R. J. *J. Phys. Chem.* **1998**, *109*, 7414.

Table 2. The Parameters of the Ellipsoidal Model and the Calculated Solvation Quantities for the Reaction in Methylene Chloride ($\epsilon_0 = 8.93$, $\epsilon_\infty = 1.875$)

	DNOA	DONA
ellipsoid parameters (Å)		
major axis	11.8	11.8
minor axis	3.59	3.59
interfocal distance	22.76	22.76
ET distance d_e	14.0	14.0
PT distance d_p	2.7	2.6
solvation energies of EVB states[a] (kcal/mol)		
ΔG^{solv} (1*a*)	−40.9 (−40.97)	−57.0
ΔG^{solv} (1*b*)	−43.5	−48.5
ΔG^{solv} (2*a*)	−57.7	−41.0 (−39.4)
ΔG^{solv} (2*b*)	−48.6 (−48.85)	−43.5
free energy differences for pairs of VB states (kcal/mol)		
$\Delta G°(1a \rightarrow 1b)$	43.1	−6.49
$\Delta G°(1a \rightarrow 2a)$	12.6	−54.2
$\Delta G°(1a \rightarrow 2b)$	10.5	−26.3
reorganization energies for pairs of VB states[b] (kcal/mol)		
$\lambda(1a \rightarrow 1b)$	0.42	0.39
$\lambda(1a \rightarrow 2a)$	35.1	35.1
$\lambda(1a \rightarrow 2b)$	31.6	39.3
$\lambda(1b \rightarrow 2a)$	39.4	31.7

[a] The solvation energies are calculated at the equilibrium proton positions corresponding to the reactant and product in the PT reaction $a \rightarrow b$. The numbers in parentheses are the results of ab initio PCM/ROHF/6-31G** calculations. [b] The reorganization energies λ do not depend on the proton position.

The two main differences between DNOA and DONA obtained from these gas phase calculations are as follows: (1) stronger electronic coupling between the two electronic states 1 and 2 for DONA due to a shorter hydrogen-bonding distance at the interface and (2) qualitatively different relative energies of the four VB states due to the oppositely directed dipoles at the interfaces for DNOA and DONA. We emphasize that solvation can significantly alter the relative energies of the four VB states. Moreover, other factors such as solvent reorganization energy and overlap of vibrational wave functions can significantly impact the mechanisms and rates.

Solvation Quantities. As discussed above and illustrated in Figure 1, we used a five-site ellipsoidal electrostatic continuum model to calculate the solvation energies and reorganization energy matrix elements. The distance d_p between the proton donor and acceptor sites was equal to the N−O distance obtained in the electronic structure calculations described above. The ellipsoidal parameters and the distance d_e between the electron donor and acceptor sites were fit to reproduce the solvation energies for the ground states calculated with a cavity determined from overlapping spheres using the version of the polarized continuum model (PCM) in Gaussian98.[25] These parameters and some of the calculated solvation quantities are presented in Table 2. Note that a comparison of the solvation energies indicates that the ellipsoidal model provides qualitatively reasonable results. Future work will utilize more sophisticated electrostatic continuum models with more physically realistic cavity shapes for the calculation of the reorganization energies. The solvation quantities given in Table 2 reflect fundamental differences between DNOA and DONA. These differences can be analyzed in terms of two-state VB models. The relative solvation energies of the VB states can be explained from purely electrostatic arguments, where greater separation of charge in a VB state leads to larger solvation energy. The total free energy (gas phase energy plus solvation energy) of each VB state i can be expressed as

$$U_i = (h_o)_{ii}(r_p^\circ) - \frac{1}{2}\int d\mathbf{r}\, \rho_{ii}(\mathbf{r})\hat{K}(\epsilon_o)\rho_{ii}(\mathbf{r}) \qquad (20)$$

where r_p° is the equilibrium position of the proton for diabatic state i and the charge densities are also evaluated at r_p°. The free energy difference between solvated VB states i and j is simply $\Delta G_{i\rightarrow j}^\circ = U_j - U_i$. These quantities are given in Table 2. For DNOA, the PT ($1a \rightarrow 1b$), ET ($1a \rightarrow 2a$), and EPT ($1a \rightarrow 2b$) reactions are endothermic, with the EPT reaction less endothermic than the ET reaction by ∼2 kcal/mol. For DONA, all three charge-transfer reactions are exothermic, with ET more exothermic than EPT by ∼28 kcal/mol. These differences suggest that, thermodynamically, DNOA favors EPT while DONA favors ET.

The reorganization energies also provide useful information about the two systems. For a two-state system involving states i and j, the reorganization energy defined in the standard two-state Marcus model[14] is

$$\lambda_{i\rightarrow j} = -\frac{1}{2}\int d\mathbf{r}[\rho_{jj}(\mathbf{r}) - \rho_{ii}(\mathbf{r})][\hat{K}(\epsilon_o) - \hat{K}(\epsilon_\infty)] \times [\rho_{jj}(\mathbf{r}) - \rho_{ii}(\mathbf{r})] \qquad (21)$$

This expression is related to the reorganization energy matrix elements in our formulation through the expression $\lambda_{1a\rightarrow i} = t'_{ii}/2$. As will be discussed below, typically the dependence of the reorganization energies on r_p is negligible. The reorganization energies for two-state VB models are given in Table 2. Note that the reorganization energy for ET is identical for the two systems due to the same values for the ellipsoidal parameters and d_e. The reorganization energy for PT is virtually identical for the two systems, with the slight difference due to the different values for d_p. The PT reorganization energies are very small due to the large size of the ellipsoidal cavity. Note that the reorganization energies are not additive; i.e., the reorganization energy for EPT is not the sum of that for PT and ET but can be expressed as

$$\lambda_{1a\rightarrow 2b} = \lambda_{a\rightarrow b} + \lambda_{1\rightarrow 2} + t'_{1b,2a} \qquad (22)$$

or the equivalent for $\lambda_{1b\rightarrow 2a}$. Also note that $t'_{1b,2a}$ is negative for DNOA and is approximately equal to $-t'_{1b,2a}$ for DONA (where the slight difference in magnitudes is due to the different values for d_p). Thus, $\lambda_{1a\rightarrow 2b}$ is smaller (larger) than $\lambda_{1\rightarrow 2}$ for DNOA (DONA). As a result, the reorganization energy for ET is larger than that for EPT for DNOA, while the reverse is true for DONA (assuming the reaction starts in state 1*a*). This

difference suggests that solvation reorganization energies favor EPT for DNOA and ET for DONA.

The values of the free energy differences and the reorganization energies obtained from two-state VB models can be used in the simple two-state Marcus expression[14] to estimate the barrier heights as

$$\Delta G^{\ddagger}_{i\rightarrow j} = \frac{(\lambda_{i\rightarrow j} + \Delta G^{\circ}_{i\rightarrow j})^2}{4\lambda_{i\rightarrow j}} \tag{23}$$

and to determine whether the reaction is in the Marcus normal or inverted region (where the Marcus inverted region is defined as $-\Delta G^{\circ}_{i\rightarrow j} > \lambda_{i\rightarrow j}$)[22,23] for the different reaction channels. For DNOA, both the ET and EPT channels are in the Marcus normal region with barriers of 16.2 and 14.0 kcal/mol, respectively. Thus, EPT is favored due to a lower barrier height. For DONA, the ET channel is in the inverted region with a barrier of 2.60 kcal/mol, while the EPT channel is in the normal region with a barrier of 1.07 kcal/mol. Again the EPT channel is favored due to a lower barrier height. The lower barrier heights for DONA suggest that the overall electron transfer rate is faster for DONA than for DNOA.

To summarize, the differences between DNOA and DONA obtained from the analysis of two-state VB models are as follows: (1) all charge transfer reactions from state 1*a* are endothermic for DNOA and exothermic for DONA; (2) thermodynamically, EPT is favored for DNOA and ET is favored for DONA (i.e. the solvated 2*b* VB state is lower than the solvated 2*a* VB state for DNOA, and the reverse is true for DONA); (3) the solvent reorganization energy is larger for ET than for EPT for DNOA, and the reverse is true for DONA; (4) both ET and EPT are in the Marcus normal region for DNOA, while the ET channel is in the inverted region and the EPT channel is in the normal region for DONA; (5) the activation energy barriers for both ET and EPT are significantly lower for DONA than for DNOA. All of these differences are due to electrostatic effects arising from the oppositely directed dipoles at the interfaces for DNOA and DONA. We emphasize that this two-state VB model analysis neglects several critical factors in PCET reactions. First, due to the large magnitudes of the couplings V^{PT1} and V^{PT2} between the two PT states *a* and *b*, these two PT states are mixed extensively in the adiabatic states. Thus, the energetics of the adiabatic states may differ significantly from those of the VB states. Second, the quantum mechanical behavior of the transferring proton leads to substantial contributions from zero-point energy and excited proton vibrational states. In particular, the overlap of the proton vibrational states for the various channels will impact the coupling strength and thus the rates.

Multidimensional Free Energy Surfaces and Approximate Rates. We calculated the two-dimensional mixed electronic/proton vibrational adiabatic free energy surfaces and the approximate rates using the methodology described above. Figure 3 depicts the two-dimensional ground state free energy surfaces for the two systems. These two-dimensional surfaces depend on two scalar solvent variables, z_p and z_e, corresponding to proton and electron transfer, respectively. The dominant VB state is indicated on the contour plots for each minimum. Note that, for DNOA, there are two minima on the ground state corresponding to the reactant (1*a*) and product (2*b*). In contrast, DONA exhibits only a single minimum on the ground state corresponding to the product (2*a*) because the 1*a* state is so much higher in energy than the 2*a* state. Moreover, for DNOA

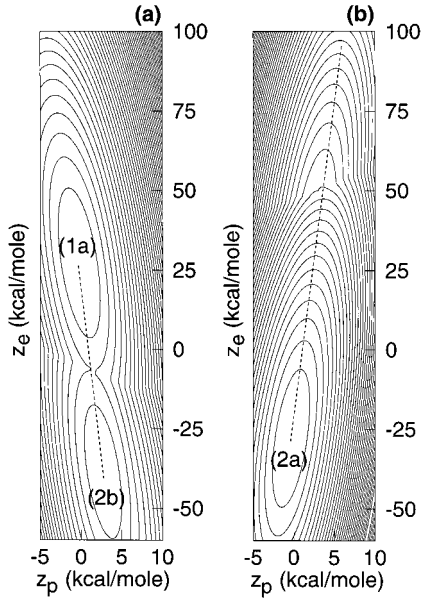

Figure 3. Two-dimensional ground state free energy surfaces for (a) DNOA and (b) DONA. The straight-line reaction paths are shown on the contour plots as dashed lines, and the minima are labeled according to the dominant VB states. Note that the scales for the ordinate and abscissa differ.

the ground state product is predominantly 2*b* (the EPT channel), while for DONA the ground state product is predominantly 2*a* (the ET channel). These observations are consistent with the two-state analysis, which suggested that for DNOA EPT is thermodynamically favored and is in the Marcus normal region, while for DONA, ET is thermodynamically favored and is in the Marcus inverted region. The straight-line reaction paths obtained by connecting the reactant and product are indicated on the contour plots as dashed lines. Figure 4 depicts slices of the two-dimensional adiabatic free energy surfaces along these straight-line reaction paths. The excited states along these reaction paths provide additional information about the reactions.

Figure 4a depicts the adiabatic states along the straight-line reaction path for DNOA, where each adiabatic state is labeled according to the dominant VB state. These results illustrate that the ET and EPT reactions are both in the Marcus normal region. The lowest energy reactant 1*b* state is more than 30 kcal/mol higher than the lowest reactant 1*a* state, indicating that the 1*b* state does not play an important role at room temperature. Moreover, the product states alternate between 2*b* and 2*a* character, with the lowest energy state having 2*b* character. The reaction mechanism can be analyzed in terms of the rate expression given in eq 13. EPT is favored by the lower barrier, which is equivalent to the term $(\Delta G^{\circ}_{mn} + \lambda_{mn})^2/(4\lambda_{mn})$ in the exponential in eq 13. On the other hand, ET is favored by the larger overlap between the proton vibrational wave functions for $1a \rightarrow 2a$ than for $1a \rightarrow 2b$. (Note that the proton vibrational states are localized near the proton donor for PT state *a* and are localized near the proton acceptor for PT state *b*.) This vibrational overlap is included in the coupling term V_{mn} in eq 13. Application of eq 13 leads to a rate constant of $8 \times 10^3\ s^{-1}$ and indicates that the four lowest product states contribute to the rate, with the largest contribution from ET to the lowest 2*a* state, the next largest contribution from EPT to the lowest 2*b* state, and the next two contributions from EPT and ET, respectively, to vibrationally excited states. Thus, both ET and EPT mechanisms are important for this system.

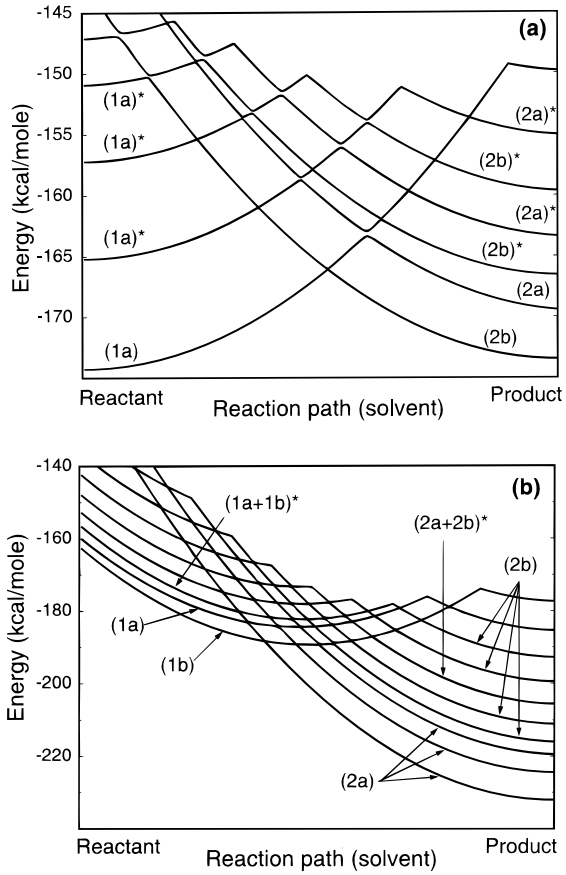

Figure 4. Slices of the two-dimensional adiabatic free energy surfaces along the reaction paths indicated in Figure 3 for (a) DNOA and (b) DONA. The adiabatic states are labeled according to the dominant VB states.

Figure 4b depicts the adiabatic states along a straight-line reaction path for DONA, where again the adiabatic states are labeled according to the dominant VB state. For DONA, the reactant 1*a* and 1*b* states are close in energy, indicating that the 1*b* state plays a significant role in this reaction at room temperature. Thus, photoexcitation may induce proton transfer prior to electron transfer. The lowest three product states have 2*a* character, and ET reactions to these states are in the inverted region. The fourth and fifth product states have 2*b* character, the sixth is a mixture of 2*a* and 2*b*, and the next two have 2*b* character. The ET and EPT reactions to these excited states are in the Marcus normal region. As for DNOA, the mechanism of this reaction can be analyzed in terms of the rate expression given in eq 13. For DONA, both ET and EPT from both the 1*a* and 1*b* reactant states are possible and are expected to be very fast due to low barriers and large overlap between the proton vibrational wave functions for $1a \rightarrow 2a$ and for $1b \rightarrow 2b$. Application of eq 13 leads to a rate constant of 1×10^{12} s^{-1} from the lowest 1*a* reactant state (which involves significant contributions from the lowest nine product states) and 2×10^{12} s^{-1} from the lowest 1*b* reactant state (which involves significant contributions from the lowest eight product states). For the reaction from the lowest 1*a* reactant state, the largest contributions to the rate constant are from the first through fifth product states, with the first through third states corresponding to 2*a* (ET) and the fourth and fifth states corresponding to 2*b* (EPT). For the reaction from the lowest 1*b* reactant state, the largest contributions to the rate constant are from the third and fourth product states, which correspond to 2*a* (EPT) and 2*b* (ET), respectively. Thus, as for DNOA, both ET and EPT mechanisms are important for DONA.

Figures 3 and 4 provide useful qualitative information concerning the relative rates of electron transfer for DNOA and DONA. As shown in eq 13, the rate decreases with barrier height and increases with coupling between the relevant states (which are mixed electronic/proton vibrational states). Our results indicate that the barriers for the dominant reactions are significantly higher in DNOA than in DONA. Moreover, the couplings between the states are smaller for DNOA than for DONA due to a larger hydrogen-bonding distance at the PT interface for DNOA (leading to slightly smaller values of V^{ET} and V^{EPT}). In addition, more reactant and product states contribute to the reaction for DONA than for DNOA. These differences indicate that the overall rate of electron transfer is larger for DONA than for DNOA, which is consistent with the experimental result. Note that the approximate rates calculated with eq 13 for DNOA and DONA differ substantially from the experimentally measured values for **1** and **2**.[5] Due to the complexity of these systems, this approximate treatment with these simplified analogues is not expected to be quantitatively accurate. Nevertheless, this theoretical analysis provides insight into the fundamental reasons for the difference in the rates for the two systems.

Conclusions

In this paper, we applied a multistate continuum theory to experimentally studied PCET reactions. In this theory, the solute is described with a multistate valence bond model, the solvent is represented as a dielectric continuum, and the active electrons and transferring proton(s) are treated quantum mechanically on equal footing. The two systems studied represent a donor−(amidinium−carboxyate)−acceptor salt bridge (DNOA) and the corresponding switched interface donor−(carboxylate−amidinium)−acceptor complex (DONA). Our calculations indicated the following differences between DNOA and DONA:

1. EPT is thermodynamically favored over ET, and the solvent reorganization energy for EPT is lower than that for ET for DNOA. In contrast, ET is thermodynamically favored over EPT, and the solvent reorganization energy for ET is lower than that for EPT for DONA. These observations are of limited significance, however, since both ET and EPT occur for DNOA and DONA due to the importance of excited product states.

2. PT does not play an important role in electronic state 1 for DNOA, while PT is expected to play an important role in electronic state 1 for DONA.

3. Only four product states contribute significantly to the rate for DNOA, while eight or nine product states contribute significantly to the rate for DONA.

4. The ET/EPT reactions are endothermic for DNOA, while the ET/EPT reactions to the lowest eight product states are exothermic (and extremely exothermic for the lower states) for DONA.

5. All ET and EPT reactions are in the Marcus normal region for DNOA, while ET reactions to the lowest three product states are in the Marcus inverted region and ET/EPT reactions to the higher states are in the Marcus normal region for DONA.

6. The activation energy barriers for the dominant reactions are higher for DNOA than for DONA.

7. The coupling between the two electronic states is smaller for DNOA than for DONA due to a larger hydrogen-bonding distance at the PT interface for DNOA.

These differences are consistent with the experimental result that the rate of PCET is faster for **2** (corresponding to DONA)

than for **1** (corresponding to DNOA). The calculations presented in this paper provide insight into the fundamental principles of PCET through asymmetric salt bridges. Future work will focus on improving the quantitative accuracy of these calculations. For example, the electrostatic effects of the Ru atom will be incorporated into the electronic structure and solvation energy calculations. Moreover, the solvation energies and reorganization energy matrix elements will be calculated with more sophisticated electrostatic continuum methods using more physically realistic cavity shapes. Another important improvement will be to treat both hydrogen atoms at the PT interface quantum mechanically within the framework of the multistate continuum theory. Furthermore, the inner-sphere reorganization will be incorporated into the multistate continuum theory by introducing a collective inner-sphere reaction coordinate that will be treated quantum mechanically in the same way as the transferring proton(s). Although these improvements are not expected to alter the qualitative conclusions of this paper, they will allow a more quantitatively accurate analysis. Future work will also center on the development of a rate expression for general PCET reactions and the application of this methodology to other types of PCET reactions.

Acknowledgment. We are grateful for financial support from the NSF CAREER program grant CHE-9623813 and the Clare Boothe Luce Foundation. S.H.-S. is the recipient of a Ralph E. Powe ORAU Junior Faculty Enhancement Award, an Alfred P. Sloan Foundation Research Fellowship, and a Camille Dreyfus Teacher-Scholar Award.

JA992380Y